Space Technology Facilitates the Preventive Monitoring and Preservation of the Great Wall of the Ming Dynasty: A Comparative Study of the Qingtongxia and Zhangjiakou Sections in China

Fulong Chen, Wei Zhou, Hang Xu, Issaak Parcharidis, Hui Lin, *Senior Member, IEEE*, and Chaoyang Fang

***Abstract*—In this study, an integrated monitoring and evaluation approach was proposed to fix the systematic safeguarding gap of the Great Wall corridor using space technologies. Two representative sections of the Great Wall located in Qingtongxia County and Zhangjiakou City in China were selected for a preliminary comparative investigation to ascertain the coupling mechanism and spatiotemporal characteristics of the driving forces for the heritage damage. The surface deformation rates were estimated by synthetic aperture radar interferometry, and the interaction between the deformation rates and the normalized difference vegetation index (NDVI) and meteorological and topographic data was calculated using the correlation matrix. The results showed the following: 1) the surface motions along the observed landscape corridor of the Great Wall were decreased in 2015–2018; 2) the correlation coefficients between the deformation rate and the elevation, slope, annual wind speed, and NDVI in Qingtongxia were 0.524, 0.115, 0.582, and 0.522, respectively, indicating the dominant influence of surface runoff and high winds on the degradation of the rammed-earth wall in the western arid regions; vice versa, 3) the correlation coefficients between the deformation rate and the aforementioned factors in Zhangjiakou were 0.065, 0.027, 0.025, and 0.052, respectively, indicating negligible effects of natural processes for the decline of Great Wall in the eastern section. This study not only provides new insights into preventive monitoring and risk assessment of the entire Great Wall but also highlights the potential of space technologies and a geographical perspective for the sustainable conservation of large-scale heritage sites.**

Manuscript received June 14, 2020; revised August 6, 2020 and September 4, 2020; accepted September 7, 2020. Date of publication September 10, 2020; date of current version September 30, 2020. This work was supported in part by the National Key Research and Development Program of China under Grant 2017YFE0134400 and in part by the National Natural Science Foundation of China (NSFC) under Grant 41771489 and Grant 41701497. *(Corresponding author: Wei Zhou.)*

Fulong Chen is with the Key Laboratory of Poyang Lake Wetland and Watershed Research, Ministry of Education, School of Geography and Environment, Jiangxi Normal University, Nanchang 330022, China, with the Key Laboratory of Digital Earth Science, Aerospace Information Research Institute, Chinese Academy of Sciences, Beijing 100094, China, and also with the International Centre on Space Technologies for Natural and Cultural Heritage under the Auspices of UNESCO, Beijing 100094, China (e-mail: chenfl@aircas.ac.cn).

Wei Zhou and Hang Xu are with the Key Laboratory of Digital Earth Science, Aerospace Information Research Institute, Chinese Academy of Sciences, Beijing 100094, China (e-mail: zhouwei@aircas.ac.cn; xuhang@radi.ac.cn).

Issaak Parcharidis is with the Department of Geography, Harokopio University of Athens, Kallithea 17671, Athens, Greece (e-mail: parchar@hua.gr).

Hui Lin and Chaoyang Fang are with the Key Laboratory of Poyang Lake Wetland and Watershed Research, Ministry of Education, School of Geography and Environment, Jiangxi Normal University, Nanchang 330022, China (e-mail: huilin@cuhk.edu.hk; fcy@jxnu.edu.cn).

Digital Object Identifier 10.1109/JSTARS.2020.3023297

***Index Terms*—Correlation measurement, cultural heritage, geographical perspective, Ming Great Wall, preventive monitoring, risk assessment, synthetic aperture radar (SAR) interferometry.**

I. Introduction

As THE largest and most extensive structure of monumental architecture in China, the Great Wall is a magnificent architectural miracle with unparalleled historical and cultural significance in human history. The Great Wall was continuously constructed in ancient China from the Warring States period (475–221 B.C.) to Qing Dynasty (1636–1912 A.D.) and has a length of tens of thousands of kilometers. The sustainable development of the Great Wall is facing considerable challenges due to natural fissures, climate change, and anthropogenic activities. However, traditional monitoring methods, such as visual inspections, are not suitable for real-time surveillance, early warning, and preventive safeguarding of cultural heritage due to low efficiency and technological limitations. Owing to the rapid development of Earth observation technology, satellite remote sensing has become increasingly important in archaeological explorations [1], [2] and preventive monitoring of heritage sites [3], [4] due to its ability to extract information objectively and quantitatively from space. Optical remote sensing, light detection and ranging (LiDAR), and imaging radar are three prevailing remote sensing approaches. Remote sensing techniques have been used widely in the field of cultural heritage since the methods are suitable for practical applications. In general, optical remote sensing is widely used in archaeological prospection [5] and dynamic monitoring of environmental parameters surrounding heritage sites [6] due to its advantages of high spatiotemporal and spectral resolution. LiDAR has been used for archaeological studies in forested areas [1], [7] and for digital heritage documentation [8], [9] due to its capability of 3-D data representation and depiction of microtopography. In contrast, imaging radar is characterized by all-weather data acquisition and subsurface penetration in arid landscapes. This technology not only extends the scope of remote sensing in archaeology in areas that are challenging to image (e.g., cloudy and rainy regions and arid and remote areas) but has also been recommended by UNESCO as an effective monitoring tool due to its ability to detect archaeological remains and determine subtle deformations (with an accuracy in the

millimeter range). Polarized and coherent microwave images and related technologies have been used, e.g., synthetic aperture radar (SAR) interferometry (InSAR).

Architectural heritage, especially ancient architecture, is an important component of tangible cultural heritage. Motion anomalies (differential deformations in the spatiotemporal domain) [10] are significant indicators used for the preventive monitoring and risk assessment of heritage properties. These anomalies indicate structural defects of architectural heritage sites and the surrounding landscape and can be obtained using multitemporal SAR interferometry (MTInSAR). This method has been increasingly used as a result of improvements in satellite image resolution and technological developments in motion estimation [11]–[15]. For instance, two-scale deformations (from the monument to the landscape) were estimated at the Angkor World Heritage site, providing new insights into the collapse of ancient temples, as well as addressing the emerging water crisis to ensure the sustainability of cultural landscapes affected by the tourism industry [3], [16].

In addition to the destruction of the Great Wall and the surrounding cultural landscape, subtle deformations in the landscape corridor of the Great Wall cause other damage, such as the collapse of parts of the monument due to the long-term movements. Due to the complexity and diversity of the natural environment and anthropogenic activities in the Great Wall corridor, it is urgent to introduce new Earth observation technologies for the preventive monitoring and preservation of this large-scale heritage site with extraordinary spatiotemporal scale (traversing China in the east–west direction, with tens of thousands of kilometers and with a history dating from B.C. to the Qing Dynasty). In this study, for the first time, the surface deformations in the corridor of the Great Wall of the Ming Dynasty (abbreviated as Ming Great Wall) in Qingtongxia County (Ningxia Hui Autonomous Region, western China) and Zhangjiakou City (Hebei Province, eastern China) were estimated using the MTInSAR approach that is adaptable for mountainous regions. The mechanisms causing damage to the defensive wall were comparatively investigated using the correlation matrix of multisource data (including terrain, land cover, and meteorological data), as well as on-site interviews and surveys. The spatiotemporal evolution of the risk factors, as well as their impacts on the Great Wall, was clarified, providing scientific data and technical solutions to fix the methodology and application gaps of space technologies for the systematic monitoring and preservation of the Great Wall, which was constructed with different materials (i.e., rammed earth in the west and stone/brick in the east) and distributed along diverse geographical environments.

II. Experimental Sites and Data

The Ming Great Wall starts in the Hushan Mountain of Liaoning Province near the Yalu River in the east and ends at Jiayuguan in Gansu Province in the west, with a total length of approximately 6300 km. It spans ten provinces (cities and autonomous regions) including Liaoning Province, Hebei Province, Beijing City, Tianjin City, Shanxi Province, Shaanxi Province, the Inner Mongolia Autonomous Region, the Ningxia Hui Autonomous Region, Gansu Province, and Qinghai Province from the east to the west, as shown in Fig. 1. The Ming Great Wall was constructed using local materials as a military defense structure and an alert system against the nomadic invasion from the northwest frontiers. Topographic features were incorporated in the route selection of the wall for defense functions and to minimize the workload of the construction project. Consequently, the wall in the eastern section is located on steep ridges and was constructed with stones and bricks. In contrast, the rammed-earth wall located in the western Loess Plateau and grassland Gobi landform was constructed using local raw materials that are strongly affected by long-term weathering and natural erosion processes. Two sections of the wall located in Qingtongxia County (Ningxia Hui Autonomous Region, China) and Zhangjiakou City (Hebei Province, China) (as marked by rectangles in Fig. 1) were selected for the preliminary investigation to analyze the impact of natural factors and anthropogenic activities on the Ming Great Wall. The section in Qingtongxia County is located at the eastern foot of Helan Mountain in western China, and it was built in the tenth year of Jiajing Period (1531 A.D.). The North Fork site (where the inner and outer wall heights are 9.7 and 8.0 m, respectively, and the top width is 3.2 m) is one of the best-preserved parts of the wall in the section from Ningxia to the Hexi Corridor. It was the paragon of the rammed-earth Great Wall and was sequentially rammed several times (i.e., both sides of the main wall were successively rammed). Zhangjiakou City is one of the most famous regions for the construction of the Great Wall of different dynasties emerged in Chinese history. The Great Wall and related architectural sites in this area were declared state-level cultural relics; therefore, this location is the "Museum" of the Great Wall of China. The Ming Great Wall in this location was constructed in the period from Yongle to Chenghua of the Ming Dynasty (1403–1487 A.D.). It is essential to conduct dynamic monitoring and sustainability evaluations of the Great Wall considering its role as a model of stone–brick construction, as well as the potential impact from infrastructure construction related to the 2022 Winter Olympic Games.

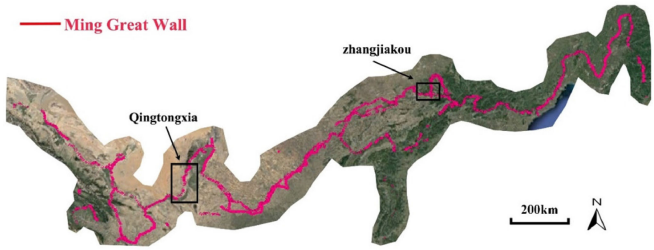

Fig. 1. Ming Great Wall in China extends in an east–west direction. The two study areas in Qingtongxia and Zhangjiakou are marked by rectangles.

The multisource spatiotemporal data used in this study include 1) Sentinel-1 time-series InSAR images acquired in 2015–2018; 2) contemporary Sentinel-2 L1C multispectral images; 3) precipitation and wind speed data from meteorological stations; 4) 3-arc Shuttle Radar Topography Mission (SRTM) digital elevation model (DEM), and annual wind speed data. Sentinel-1 is an Earth observation satellite of the European Space Agency's Copernicus program, which was previously called the Global Monitoring for Environment and Security program. Sentinel-1 consists of two satellites (A/B) and carries C-band SAR. The

TABLE I
DETAILS OF THE SENTINEL-1 IMAGES ACQUIRED IN 2015–2018

Sections	Polarization	Observation period/scenes	Ground resolution
Qingtongxia	VV or VV/VH	2015/07~2016/09 19 scenes 2017/03~2018/05 33 scenes	20 m
Zhangjiakou	VV or VV/VH	2015/07~2016/12 22 scenes 2017/01~2018/05 39 scenes	20 m

ground resolution of the interferometric wide swath (IW), single look complex (SLC), single-polarization (VV), or cross-polarization (VV/VH) data[1] is approximately 20 m, as listed in Table I. Precipitation/wind speed data for the observation period of 2015–2018 were obtained from meteorological stations in the vicinity of the study sites[2] (Fig. 2). Multispectral images of Sentinel-2 (12 bands including red–green–blue and near-infrared) were collected for the calculation of the normalized difference vegetation index (NDVI) [17] of the landscape corridor. The spatial resolution of the visible and near-infrared bands is 15 m. The annual average wind speed data (1 km spatial resolution, interpolated from 740 meteorological stations in China in the period of 1961–2000) were obtained from the service platform of the National Ecological Science Data Center.[3]

III. METHODOLOGY AND DATA PROCESSING

An integrated monitoring and evaluation method based on space technologies was proposed to determine the interactions and mechanisms of the factors causing motion anomalies along the landscape corridor of the Ming Great Wall. The approach utilized remote sensing information for spatiotemporal analysis of the driving forces, taking advantage of the macro observation capability of the satellites (Fig. 3) in order to fix the systematic safeguarding gap of the large-scale linear heritage. The integrated solution with following steps was used in the analysis: 1) The mountain-terrain adaptable small baseline subset (SBAS) method was utilized to calculate the linear motion rates of the surface in the landscape corridor; 2) multispectral remote sensing images were used for the generation of the NDVI for the land cover characterization; 3) multisource thematic data, such as meteorological, terrain, and NDVI data, were used in a spatial correlation analysis to determine the relationships between the surface motion and the factors causing wall damage. This study provided a pilot demonstration for the preventive monitoring and conservation of the Great Wall corridor through the methodology adaption and technology integration.

A. *MTInSAR for Deformation Estimation*

The mountain-terrain adaptable SBAS approach was utilized to improve the spatial density of the measurement points and

[1][Online]. Available: https://scihub.esa.int
[2][Online]. Available: https://www.worldweatheronline.com/
[3][Online]. Available: http://www.cnern.org.cn/

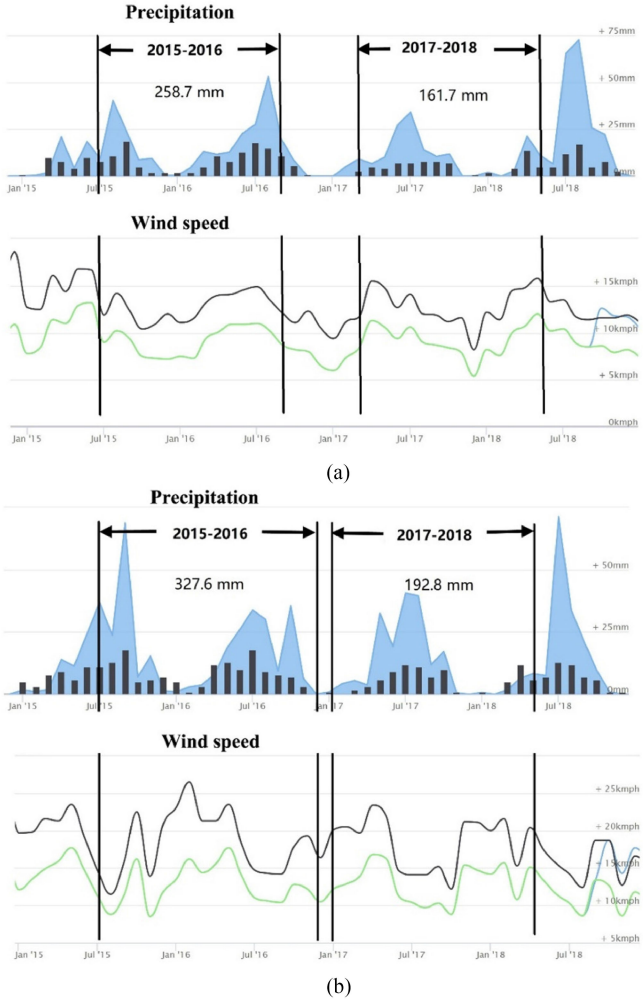

Fig. 2. Precipitation and wind speed data for the period of 2015–2018 were obtained from meteorological stations in the vicinity of (a) Qingtongxia County and (b) Zhangjiakou City. The overlap in time with the InSAR observations is marked by the arrows.

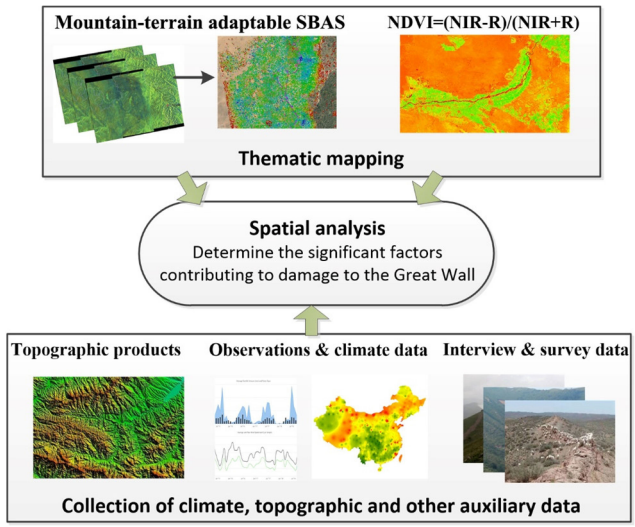

Fig. 3. Schematic diagram of the preventive monitoring of the landscape corridor and the analysis of the factors causing damage to the Ming Great Wall.

obtain a reliable deformation inversion in the complex landform. It consisted of following steps. 1) The quality of the interferograms was improved to suppress the burst-phase jump (which is a frequent occurrence in Sentinel-1 IW interferograms) and atmospheric phase linked to the topography. That is, apart from the applied enhanced spectral diversity algorithm in the image coregistration [18], the stratified atmospheric phase error in interferograms was removed using simulated products from the generic atmospheric correction online service (GACOS) for InSAR [19], making the corrected interferograms adaptable in mountainous landforms. 2) We used the SBAS approach [11], [20] to obtain the surface deformation in the natural landscape with high density of motion measurements of the targets while preserving the coherence of interferograms.

Several interferogram subsets were generated using the predefined threshold of the small baselines. The SBAS strategy minimizes spatiotemporal decorrelation; therefore, this method is well suited for surface deformation estimation in a natural landscape. The principle of the SBAS method can be summarized as follows. We assume that M interferograms are obtained using N SAR acquisitions based on the SBAS strategy. After the removal of the flat and topographical phases, differential interferograms are generated. Spatial filters are used for phase and artifact suppression to avoid phase unwrapping errors. Consequently, the unwrapped phase at point $(x,\ r)$ of the i interferogram obtained from the master imagery acquired at time t_B and the slave imagery acquired at time t_A is defined as

$$\begin{aligned}\delta\varphi_i =\ & \varphi(t_{\mathrm{B}},x,r)-\varphi(t_{\mathrm{A}},x,r)\\ \approx\ & \frac{4\pi}{\lambda}\left[d(t_{\mathrm{B}},x,r)-d(t_{\mathrm{A}},x,r)\right]+\frac{4\pi}{\lambda}\frac{B_{\perp i}\Delta z}{R\sin\theta}\\ & +\left[\varphi_{\mathrm{atm}}(t_{\mathrm{B}},x,r)-\ \varphi_{\mathrm{atm}}(t_{\mathrm{A}},x,r)\right]+\Delta n_i \end{aligned} \quad (1)$$

where $i\ =\ 1,2,\ldots,M$; θ denotes the central incidence angle of the SAR acquisitions. $\frac{4\pi}{\lambda}[d(t_{\mathrm{B}},x,r)-d(t_{\mathrm{A}},x,r)]$, $\frac{4\pi}{\lambda}\frac{B_{\perp i}\Delta z}{R\sin\theta}$ denotes the deformation and residual height phase components, respectively. $[\varphi_{\mathrm{atm}}(t_{\mathrm{B}},x,r)-\ \varphi_{\mathrm{atm}}(t_{\mathrm{A}},x,r)]$ denotes the atmospheric phase delay, and Δn_i denotes the noise error component.

By eliminating the noise error, the phases at the observed points are defined as

$$\boldsymbol{D}\boldsymbol{v}+\boldsymbol{C}\cdot\Delta z\ =\ \Delta\boldsymbol{\varphi} \quad (2)$$

where $\boldsymbol{D}$ is the temporal matrix with the dimension of $M\times(N-1)$; $D\ (j,k)=t_k\ -t_{k-1}$ denotes the generated interferograms with small baselines, and vice versa for the no interferograms cases $D\ (j,k)=\ 0$. $\boldsymbol{v}^{\mathrm{T}}=[v_1=\frac{\varphi_2}{t_2-t_1},\ldots v_n=\frac{\varphi_N-\varphi_{N-1}}{t_N-t_{N-1}}]$ is the velocity vectors of the SAR acquisitions. $\boldsymbol{C}\ (M\times 1)=[\frac{4\pi}{\lambda}\frac{B_{\perp 1}}{R\sin\theta},\cdots\frac{4\pi}{\lambda}\frac{B_{\perp M}}{R\sin\theta}]$ is the vector of the height frequency, and Δz denotes the residual height rectified from the reference DEM data (e.g., the SRTM DEM). In the calculation of the unknown parameters (including motion and height), the least squares method or singular value decomposition is used, according to the full rank or rank deficiency condition of matrix $\boldsymbol{D}$. Nonlinear deformations and residual atmospheric phase delay can be further isolated using spatiotemporal filters and considering the spatiotemporal characteristics; for instance, atmospheric artifacts generally are low frequency in space and high frequency in time.

B. Calculation of NDVI

The NDVI, which is calculated using multispectral remote sensing data [see (3)], is an important index used for monitoring vegetation growth, estimating vegetation cover, and compensating for changes in radiometric conditions

$$\mathrm{NDVI}=(\mathrm{NIR}-R)\,/\,(\mathrm{NIR}+R) \quad (3)$$

where NIR is the reflection value of the near-infrared band; R is the reflection value of the red band. NDVI $\in[-1,1]$. A negative value indicates clouds, water, or snow, which strongly reflects visible light; zero indicates rock or bare soil, where NIR and R are approximately equal. A positive value indicates the presence of vegetation; the NDVI value increases with an increase in the density of vegetation. In this study, the NDVI was used to estimate the vegetation cover in the landscape corridor of the Great Wall, as well as to identify areas (e.g., mining and unstable slopes) of potential geohazards. These areas had low NDVI values and were verified using field visits.

C. Correlation Measurements

The spatial correlation of the influence factors was determined to understand the impact of natural processes and anthropogenic activities on the Great Wall. Multisource thematic layers of the landscape corridor were analyzed. The correlation of the spatial layers was determined using a correlation matrix and the following principle.

The covariance matrix of layers i and j with geometrical overlap is defined as

$$\mathrm{Cov}_{i,j}=\frac{\sum_{k=1}^{N}(Z_{i,k}-\mu_i)(Z_{j,k}-\mu_j)}{N-1} \quad (4)$$

where $Z_{i,k}$ and $Z_{j,k}$ are the element values of layers i and j, and N is the number of elements in the layer. μ_i and μ_j are the mean values of the layers. The elements of the covariance matrix are related to the corresponding elements of layers i and j; consequently, the correlation matrix is used instead to normalize the correlation between the layers

$$[\mathrm{Corr}_{i,j}]\ =\ \left[\frac{\mathrm{Cov}_{i,j}}{\sigma_i\sigma_j}\right] \quad (5)$$

where σ_i and σ_j are the standard deviations of layers i and j. The elements of the matrix ***Corr*** represent the correlation coefficient, with values ranging from -1 to 1.

IV. Validation of InSAR Deformation Measurements

As a quantitative index, the accuracy of InSAR deformation measurements is essential for a time-series comparison of surface deformations, as well as the correlation analysis of the different influence factors. GPS and precise leveling are accepted methods for the cross-validation of InSAR measurements. However, since there is a lack of geodetic data in remote areas, the cross-comparison of measurements from different MTInSAR algorithms using a uniform radar dataset can be applied as a

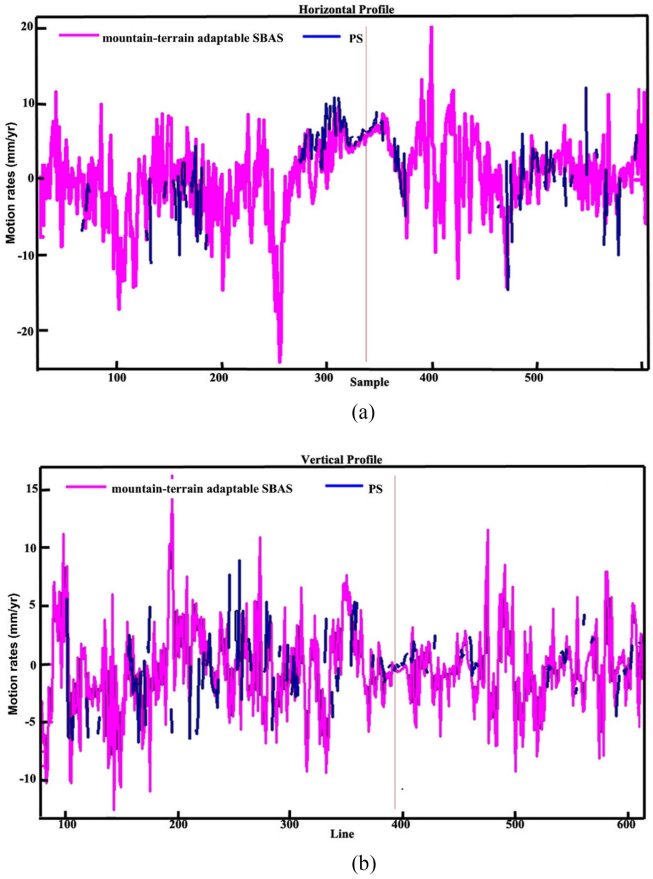

Fig. 4. Comparison of deformation measurements obtained from the mountain-terrain adaptable SBAS and PSInSAR approaches. Consistent deformations (in the range from 0 to 5.0 mm) were observed in the (a) horizontal and (b) longitudinal profiles.

tradeoff. Numerous case studies have demonstrated that the accuracy of estimated displacements of MTInSAR is at the millimeter level, especially for linear deformation rates [12], [21]. Compared with other MTInSAR approaches, the accuracy of the deformations at reliable persistent scatterer (PS) points can be guaranteed [12] when a rigorous threshold of the ensemble temporal coherence is used (e.g., higher than 0.75). Therefore, the deformations obtained from the mountain-terrain adaptable SBAS approach in this study were cross-validated using the persistent scatterer SAR interferometry (PSInSAR) method [12], as shown in Fig. 4. Consistent motion measurements in selected horizontal and longitudinal profiles were obtained, with deviations ranging from 0 to 5.0 mm. In addition, the SBAS provided a high spatial density of deformation measurements, demonstrating the applicability of this method in natural landscapes.

V. Results and Interpretations

Two observation periods (2015–2016 and 2017–2018) on the representative sections of the Ming Great Wall (Qingtongxia in the west and Zhangjiakou in the east) were used for the temporal comparison of the deformation anomalies on an interannual scale. The driving forces of the damage were identified by

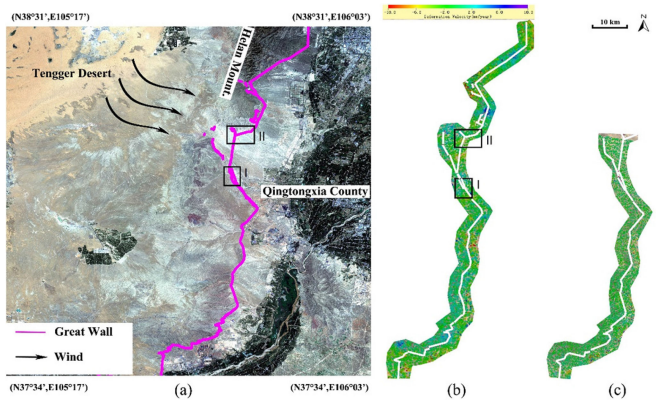

Fig. 5. Landscape corridor of the Ming Great Wall and the InSAR surface deformations in the Qingtongxia section, China. (a) Location of the Great Wall overlaid on the Sentinel-2 imagery. Annual surface deformation rates in the observation periods of (b) 2015–2016 and (c) 2017–2018. "I" indicates the hotspot with significant runoff erosion and "II" indicates the location of the North Fork site. Great Wall routes were marked by white lines in (b) and (c).

performing a spatiotemporal analysis using multiple layers of surface deformation (InSAR estimated in the observation periods of 2015–2016 and 2017–2018) and other contemporaneous geographical thematic layers of NDVI, elevation, slope, and annual wind speed.

The InSAR data processing and motion inversion were implemented by using the software tool of generic InSAR analysis toolbox [22]. The stratified atmospheric phase errors on individual interferograms (that is significant on mountain areas) were corrected using the self-developed Python toolkit and the GACOS modeling data.

Two Sentinel-2 L1C multispectral images, covering the study sites of Qingtongxia and Zhangjiakou, respectively, were collected for the NDVI product generation. Those images, acquired in 2018, were processed using the Sentinel application platform provided by the European Space Agency. The terrain-related layers of elevation and slope were generated from the 3-arc SRTM DEM data, and the annual-averaged wind speed layers were downloaded from the service platform of the National Ecological Science Data Center.[4]

A. Qingtongxia Section

Information on the natural and anthropogenic factors affecting the preservation of the Great Walls was obtained from the field interviews and surveys. For instance, the wall has been affected by cattle and sheep that are grazed in this area. V-shaped channels are common and cause significant damage to rammed-earth walls due to heavy rainfall in summer. In addition, owing to the arid climate of the Tengger Desert, a northwest wind prevails in this area (Fig. 5). The wind and dust particles have a strong weathering effect on the rammed-earth wall, resulting in significant degradation of the Great Wall due to long-term wind erosion.

Nonetheless, the quantitative effects of surface runoff and strong wind erosion on the degradation of the Ming Great Wall

[4][Online]. Available: http://www.cnern.org.cn/

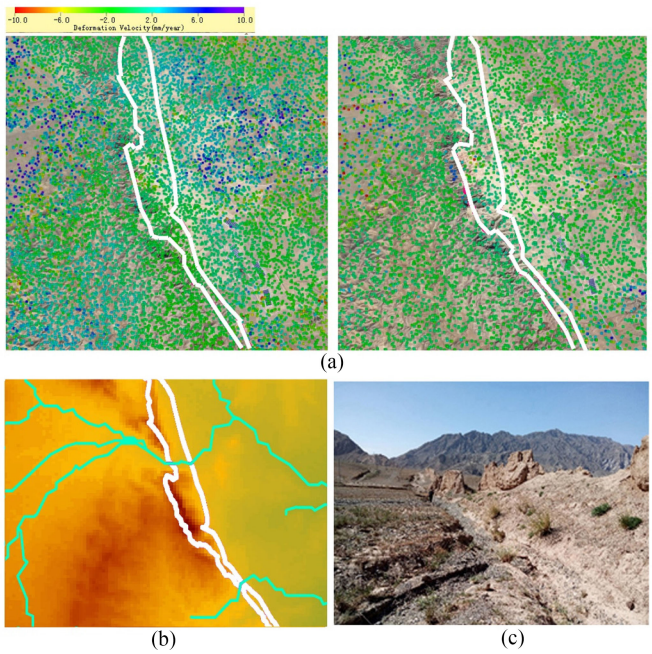

Fig. 6. Surface deformation caused by water erosion in the landscape corridor of the Ming Great Wall in Qingtongxia County, China. (a) Comparison of estimated deformation rates in the periods of 2015–2016 and 2017–2018 at "I," (b) local drainages (in green) extracted by analyzing SRTM DEM data using the ArcGIS hydrological toolkit, (c) *in situ* photo of surface runoff erosion. Great Wall routes were marked by white lines in (a) and (b).

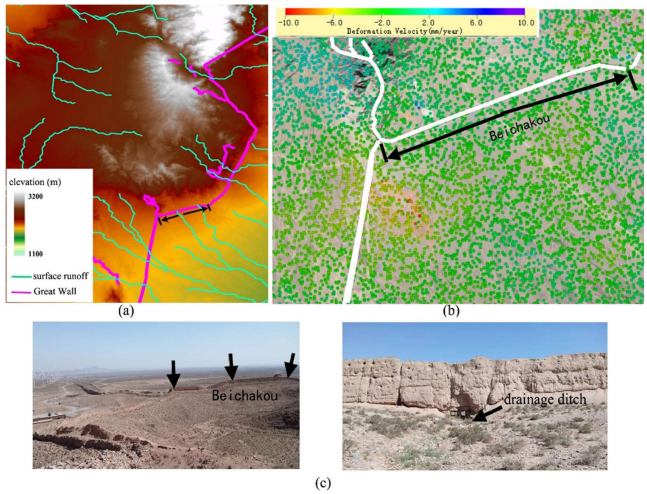

Fig. 7. Well-preserved portion of the Great Wall at the North Fork site in Qingtongxia County, China. (a) Topography and hydrology in the Great Wall corridor, the surface runoff (in green) was obtained by analyzing SRTM DEM data using the ArcGIS hydrological toolkit. (b) Estimated deformation rates in area "II" in the period of 2015–2016 with the Great Wall route marked by white lines. (c) Rammed-earth construction of the Great Wall with a drainage ditch (field photos).

in the west (e.g., Qingtongxia section) remain unclear, and a sustainability assessment has not been conducted due to the lack of scientific observation data. Therefore, the line-of-sight annual deformation rates were estimated in the observation periods of 2015–2016 and 2017–2018 along the Qingtongxia Great Wall using the adapted SBAS InSAR approach [Fig. 5(b) and (c)]. Two areas (marked by I and II) with the measured annual deformation rates were selected for a detailed analysis (Fig. 5) using the precipitation and wind speed data (Fig. 2) from the meteorological station in the vicinity. The catchment drainage in areas I and II was obtained using the 3-arc SRTM DEM data and the ArcGIS hydrological toolkit.

Area I was located in a typical catchment area with significant surface runoff indicated by the local drainage (derived by analyzing 3-arc SRTM DEM data using the ArcGIS hydrological toolkit [Fig. 6(b)] and field photos [Fig. 6(c)]. The comparison of the annual deformation rates between the observation periods of 2015–2016 and 2017–2018 indicated that the surface in this zone had experienced a mild uplift (more than +6 mm/year) caused by the soil deposit accumulation, which stabilized [Fig. 6(a)] due to a decrease in total rainfall (a decrease from 258.7 mm in 2017–2018 to 161.7 mm in 2015–2016) [Fig. 2(a)]. The effect of wind erosion was relatively negligible in several years, in particular considering the consistent wind speeds in the two interannual observation periods [Fig. 2(a)]. This result indicated the dominant impact of surface runoff on the stability of the rammed-earth wall and surrounding landscape interannually. In contrast, the wall at the North Fork site [area II in Fig. 5(a)] was intact. The analysis of the effects of topography, hydrology, and surface motions on the wall showed that the terrain in this subzone was generally gentle, and there were few areas with surface runoff compared to the surroundings [Fig. 7(a)]. In addition, there was little wind erosion of the wall due to the high mountain in the northwest [Fig. 7(a)]. The surface deformation measurements derived from InSAR at the North Fork site were relatively stable (−2 mm/year to +2 mm/year) in the observation period of 2015–2016 [Fig. 7(b)]. Except for the unique natural conditions described above, drainage ditches were used in the construction of the Great Wall [Fig. 7(c)], further minimizing erosion from surface runoff in rainy seasons.

The correlation coefficients between the surface deformations and the elevation, slope, annual wind speed, and NDVI were 0.524, 0.115, 0.582, and 0.522, respectively (Fig. 8). It was found that the Great Wall in the arid area (western China) was affected by topography-related runoff erosion, land cover, as well as wind erosion. The contributions of the different factors were similar; however, the time scale of the impacts was variable, ranging from an interannual scale for surface runoff to long-term for wind erosion [23] (although the interannual contribution of the wind erosion is negligible as aforementioned). Since the thematic data had different spatial resolutions [NDVI (15 m) > InSAR ($2^{\times}8$ multilooked in the azimuth and range direction, resulted into the spatial resolution of 40 m) > terrain (90 m) > wind speed (1 km)], the correlation coefficients only provide a general overview of the influencing factors in the corridor. Unmanned aerial vehicle-based terrain modeling and high-resolution weather data (e.g., collected by sensors linked to the Internet of Things) should be obtained to determine the detailed coupling mechanism of the driving factors.

B. Zhangjiakou Section

In contrast to the rammed-earth wall in Qingtongxia County (western China), the Ming Great Wall in Zhangjiakou City

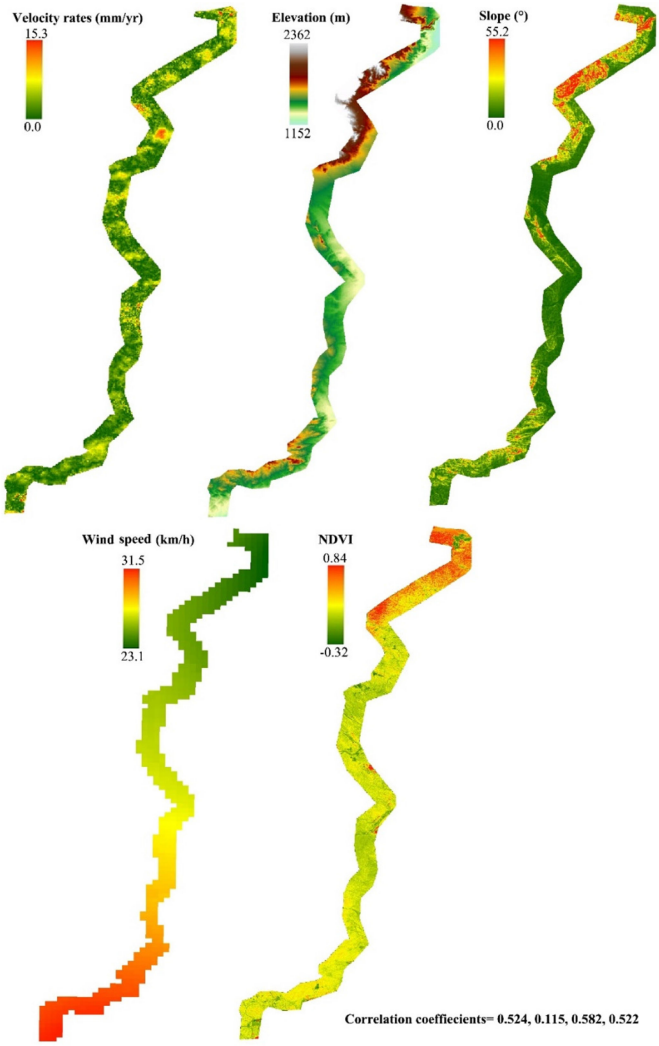

Fig. 8. Maps of the InSAR-derived deformation, elevation, slope, wind speed, and NDVI with the calculated correlation coefficients between the deformation and the aforementioned natural factors in the landscape corridor of the Ming Great Wall in Qingtongxia County, China.

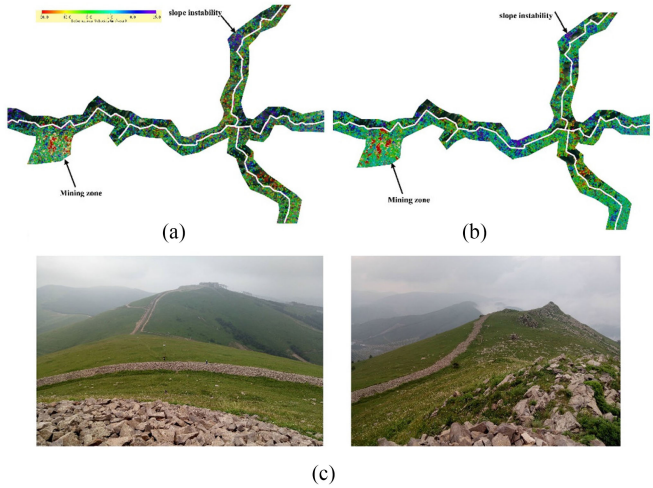

Fig. 9. Surface deformation of the Ming Great Wall in Zhangjiakou City, China in (a) 2015–2016 and (b) 2017–2018 with wall routes marked by white lines. (c) Photos of the masonry walls and the surrounding landscape.

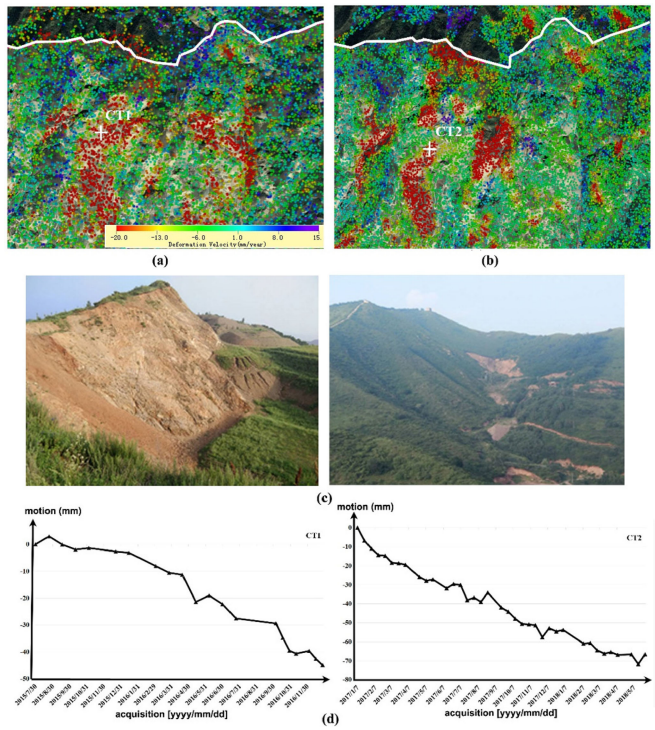

Fig. 10. Surface instability influenced by past mining activities in the area around the Ming Great Wall in Zhangjiakou City, China. Surface deformation rates in (a) 2015–2016 and (b) 2017–2018. (c) Photos of historic mining activities. (d) Deformation time series of selected point measurements of CT1 in (a) and CT2 in (b). Great Wall routes were marked by white lines.

(eastern China) was constructed with stones and bricks on the mountain ridges for defense purposes. Field investigations of the wall material and the precipitous terrain indicated that the Ming Great Wall in the Zhangjiakou section was primarily affected by mining, construction, and slope instability.

The annual surface deformation rates in the landscape corridor of the Great Wall corridor in the period of 2015–2016 and 2017–2018 are shown in Figs. 9 and 10. The deformation rates indicated that the surface of the 65-km-long monitored corridor was relatively stable. However, there were also location spots with significant surface deformations related to anthropogenic activities (mining) and unstable slopes, as marked by the arrows in Fig. 9. The measured annual deformation rate in this section ranged from −20 mm/year to +15 mm/year. Note that mining activities were prohibited before the observation period of 2015–2016 (obtained from field interviews). However, significant deformations were observed near the historic mining area due to extensive impacts on the landscape, as shown in Fig. 10. The spatial differences in the deformation rates between the two periods of 2015–2016 (ascending SAR data) and 2017–2018 (descending SAR data) surrounding the historic mining region were determined by the difference of imaging orbits and observations of the deformation trends over time.

The surface deformation rates in 2015–2016 and 2017–2018 were interpolated using universal kriging [24], as shown in

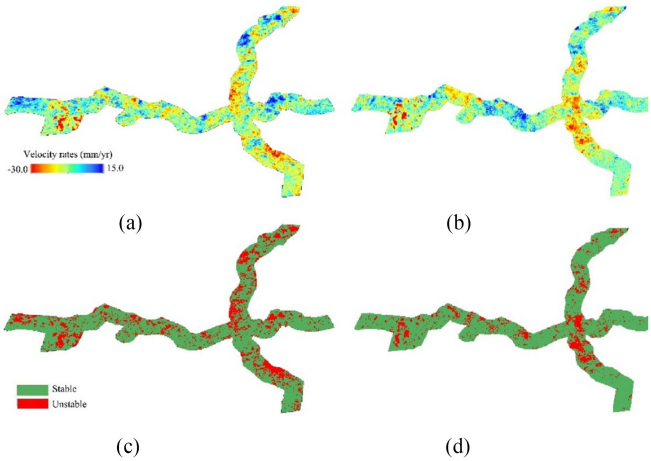

Fig. 11. Stability of the Ming Great Wall in Zhangjiakou City, China. (a) Deformation maps in 2015–2016 and (b) 2017–2018 based on universal kriging interpolation. Binary classification map of stable and unstable areas in (c) 2015–2016 and (d) 2017–2018.

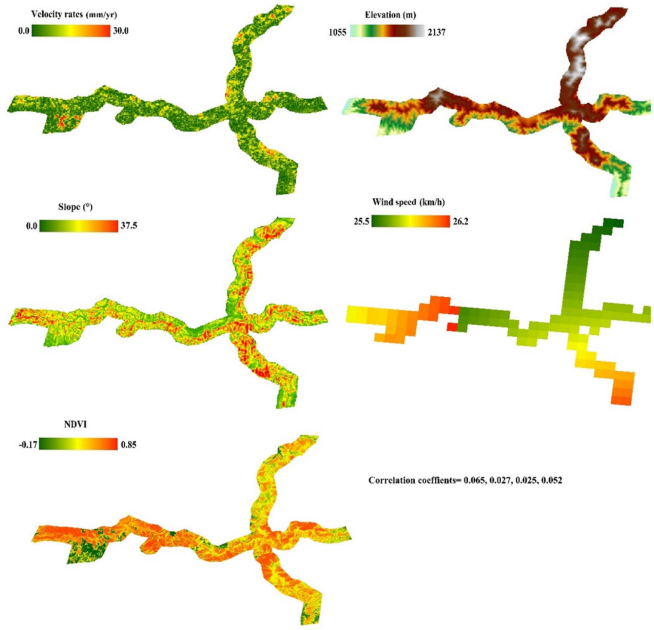

Fig. 12. Maps of the InSAR-derived deformation, elevation, slope, wind speed, and NDVI with the calculated correlation coefficients between the deformation and the aforementioned natural factors in the landscape corridor of the Ming Great Wall in Zhangjiakou City, China.

Fig. 11(a) and (b). Thematic maps of stable and unstable areas were generated using a threshold of 10 mm/year (twice the value used for the accuracy validation, Section IV) [Fig. 11(c) and (d)]. The results indicated a coupling effect of the deformations in the two periods, suggesting that the persistence and hysteresis of natural processes (dominated by geological conditions) and anthropogenic disturbances over time contributed to surface instability. The proportions of unstable areas in the corridor in 2015–2016 and 2017–2018 were 22.8% and 14.7%, respectively, showing a decrease of 8.1%. This result was partially attributed to a decline in the rainfall [decreasing from 327.6 mm in 2015–2016 to 192.8 mm in 2017–2018, as shown in Fig. 2(b)] and the resulting decrease in the movement of the unstable slopes. In addition, the prohibition of anthropogenic disturbances, such as mining, benefitted the sustainable conservation of the Ming Great Wall in Zhangjiakou. The impacts of topography, annual wind speed, and land cover on the surface stability were quantitatively evaluated. The spatial correlations between the factors and the InSAR deformations were investigated. The absolute values of the correlation coefficients between the deformation rates and the elevation, slope, annual wind speed, and NDVI were 0.065, 0.027, 0.025, and 0.052, respectively (Fig. 12). These values indicated that the effect of these factors on the surface stability and the Great Wall were negligible in the mountainous corridor. However, the anthropogenic activities had a significant impact on the Great Wall [e.g., mining activities, as shown in Fig. 10(c)], thereby adversely affecting conservation efforts in this area.

C. Comparison of the Driving Forces for the Heritage Damage

Different from the manageable anthropogenic activities, the natural factors for the damage of heritage sites are generally uncontrollable. In this study, the natural factors of terrain, annual wind speed, and land cover for the motion anomaly and potential damages of the Great Wall along the cultural corridor of Qingtongxia and Zhangjiakou were comparatively analyzed (Fig. 13) in order to understand their influence patterns quantitatively.

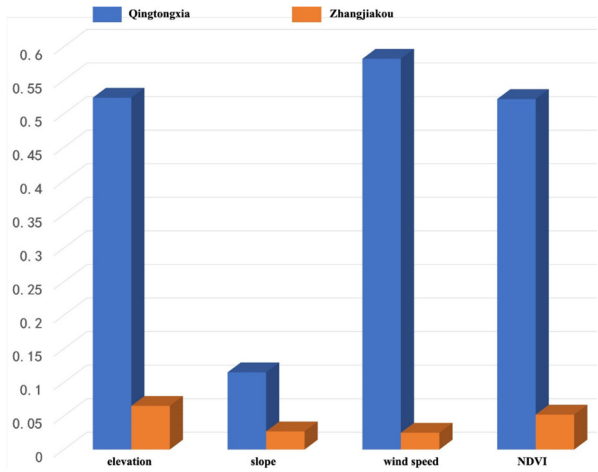

Fig. 13. Comparison of the calculated correlation coefficients of geographical thematic layers between the Great Wall landscape of Qingtongxia and Zhangjiakou, China.

Diverse patterns were observed in the comparative experiment, implying the determining factors of the constructed monument materials as well as the hosting geographical environment. Generally, the rammed-earth wall is more prone to the erosion of interannual catchment floods and/or long-term high winds compared with stone–brick wall monuments. The temporal variation of deformation rates indicated that the proportion of significant moving points (with the absolute value higher than 5 mm/year, that is the value used for the accuracy validation in Section IV) in the Qingtongxia section of Ming Great Wall in the western China decreased from 5.6% in 2015–2016 to 1.5%

in 2017–2018, which was attributed to the mitigated erosion of surface runoff because of the reduced precipitation. Moreover, the occurrence of wall monuments in the geographical environment with a catchment terrain and a sparse vegetation cover (low NDVI values) maximizes the surface runoff erosion for the rammed-earth wall. This evidence was verified by the calculated high correlation coefficients (>0.5) between the InSAR deformation rates and the selected natural factors (Fig. 8) of the elevation and NDVI (dominant factors linked to the surface runoff). In contrast, natural influences aforementioned for the damage of Great Wall in the Zhangjiakou section (stone–brick walls located along mountain ridges in the eastern China) were generally negligible indicated by the calculated correlation coefficients lower than 0.1 (Fig. 12). Nonetheless, the magnitude of measured deformation rates in this area (primary in the range of -20 mm/year to $+15$ mm/year) was more intense than the Qingtongxia section (primary in the range of -15 mm/year to $+10$ mm/year) due to following interpretations: 1) Slope instabilities and rapid movements are primarily caused by vulnerable topographic features and historic mining activities in Zhangjiakou; vice versa, the impact of aforementioned factors is negligible in the latter section. 2) Gradual movements in temporal are prevailing in Zhangjiakou, even on evident moving points, as shown in Fig. 10(d); in contrast, the decorrelation occurs in Qingtongxia in the case of instant runoff floods, resulting in the loss of evident deformation measurements.

In summary, the macroscopic driving forces causing the damage of Ming Great Wall throughout the east–west China were obtained in the aforementioned comparative analysis, providing informative precursors for the preventive safeguarding of the linear heritage with extraordinary spatial scale.

VI. Conclusion and Perspectives

The dynamic monitoring and sustainable conservation of the Great Wall (a symbol of the Chinese national spirit and architectural heritage monument with a linear structure) call for innovative information technologies, such as satellite remote sensing [25], [26]. Due to the advantages of wide coverage, near real-time observations, and high-precision deformation inversion, spaceborne InSAR technologies play an increasingly important role in the assessment of geological conditions and architectural heritage of the Great Wall corridor. Given the diversity of the environmental conditions, such as climate, topography, hydrology, and the construction materials, two representative sections of the Ming Great Wall in Qingtongxia County in the west and Zhangjiakou City in the east of China were investigated in detail to determine the factors contributing to the damage of the Great Wall. The spatiotemporal correlation analysis of the relationship between the surface deformation and the different factors provided new insights into the safeguarding and sustainable conservation of this large-scale architectural heritage, as well as the surrounding landscape.

The results of the case study indicated the following. 1) In the eastern section of the Ming Great Wall, which is located in mountainous terrain and was constructed using stone/bricks, the surface stability in the cultural landscape corridor was almost unaffected by the natural factors, i.e., the topography, wind speed, and land cover. In contrast, human disturbances, such as mining, had a notable impact on the deformations on the interannual scale. For example, the control of mining activities did not exacerbate the surface instability in the corridor. The proportion of unstable areas in the Zhangjiakou section decreased by 8.1% from 2015–2016 to 2017–2018. 2) The rammed-earth portion of the Great Wall in western China exhibited erosion by natural processes, such as surface runoff and wind on interannual and long-term scales, respectively. The correlation coefficients between the environmental factors and the surface deformation rates were higher than 0.5 in the Qingtongxia area, indicating the dominant influence of the natural environment on the decline of the Great Wall in this area. It should be noted that the elaborated rammed-earth wall construction method facilitates the preservation of the Great Wall. For example, the drainage ditch at the North Fork site reduced the risk of erosion and destruction of the wall due to surface runoff. As a result, the wall in this area remains intact even after six hundred years.

Complex changes occur in cultural heritage sites in time and space, especially in large-scale linear structures (such as Ming Great Wall investigated in this study) [25]. The changes depend on the nature of the monument, as well as environmental and anthropogenic influences in the landscape corridor. Consequently, it is necessary to use Earth observations and consider the geography of an area for the sustainable conservation of large-scale cultural heritage sites, especially in the Big Data era. The spatial distribution and temporal evolution of the natural and anthropogenic influencing factors can be systematically investigated using an interdisciplinary approach to heritage conservation (for the preservation of the unique value of the structure) from data acquisition, information extraction, and analysis to scenario prediction. In a future study, we will focus on the assessment of the entire Ming Great Wall in the 6300 km corridor using customized MTInSAR monitoring approaches (i.e., the parallel SBAS approach [27]) and sophisticated assessment models that incorporate big Earth data and a geographical perspective.

Acknowledgment

The authors would like to thank the European Space Agency for providing the Sentinel-1 data. They also thank the anonymous reviewers for their helpful comments and suggestions.

References

[1] A. F. Chase, D. Z. Chase, C. T. Fisher, S. J. Leisz, and J. F. Weishampel, "Geospatial revolution and remote sensing LiDAR in Mesoamerican archaeology," *Proc. Nat. Acad. Sci.*, vol. 109, no. 32, pp. 12916–12921, 2012.

[2] L. Luo *et al.*, "Airborne and spaceborne remote sensing for archaeological and cultural heritage applications: A review of the century (1907–2017)," *Remote Sens. Environ.*, vol. 232, 2019, Art. no. 111280.

[3] F. Chen *et al.*, "Radar interferometry offers new insights into threats to the Angkor site," *Sci. Adv.*, vol. 3, 2017, Art. no. e1601284.

[4] W. Xiao *et al.*, "Geoinformatics for the conservation and promotion of cultural heritage in support of the UN Sustainable Development Goals," *ISPRS J. Photogrammetry Remote Sens.*, vol. 142, pp. 389–406, 2018.

[5] R. Lasaponara, G. Leucci, N. Masini, R. Persico, and G. Scardozzi, "Towards an operative use of remote sensing for exploring the past using satellite data: The case study of Hierapolis (Turkey)," *Remote Sens. Environ.*, vol. 174, pp. 148–164, 2016.

[6] G. Jorayev, K. Wehr, A. Benito-Calvo, J. Njau, and I. Torre, "Imaging and photogrammetry models of Olduvai Gorge (Tanzania) by unmanned aerial vehicles: A high-resolution digital database for research and conservation of early stone age sites," *J. Archaeological Sci.*, vol. 75, pp. 40–56, 2016.
[7] M. A. Canuto *et al.*, "Ancient lowland Maya complexity as revealed by airborne laser scanning of northern Guatemala," *Science*, 2018, vol. 361, no. 6409, 2018, Art. no. eaau0137.
[8] F. Zhang *et al.*, "Texture reconstruction of 3D sculpture using non-rigid transformation," *J. Cultural Heritage*, vol. 16, no. 5, pp. 648–655, 2015.
[9] L. Wilson, A. Rawlinson, A. Frost, and J. Hepher, "3D digital documentation for disaster management in historic buildings: Applications following fire damage at the Mackintosh building, the Glasgow school of art," *J. Cultural Heritage*, vol. 31, pp. 24–32, 2018.
[10] F. Pratesi, D. Tapete, G. Terenzi, C. D. Ventisette, and S. Moretti, "Rating health and stability of engineering structures via classification indexes of InSAR persistent scatterers," *Int. J. Appl. Earth Observ. Geoinform.*, vol. 40, pp. 81–90, 2015.
[11] P. Berardino, G. Fornaro, R. Lanari, and E. Sansosti, "A new algorithm for surface deformation monitoring based on small baseline differential SAR interferograms," *IEEE Trans. Geosci. Remote Sens.*, vol. 40, no. 11, pp. 2375–2383, Nov. 2002.
[12] A. Ferretti *et al.*, "Submillimeter accuracy of InSAR time series: Experimental validation," *IEEE Trans. Geosci. Remote Sens.*, vol. 45, no. 5, pp. 1142–1153, May 2007.
[13] L. Zhang *et al.*, "Mapping ground surface deformation using temporarily coherent point SAR interferometry: Application to Los Angeles Basin," *Remote Sens. Environ.*, vol. 117, pp. 429–439, 2012.
[14] G. Fornaro, S. Verde, D. Reale, and A. Pauciullo, "CAESAR: An approach based on covariance matrix decomposition to improve multibaseline multitemporal interferometric SAR processing," *IEEE Trans. Geosci. Remote Sens.*, vol. 53, no. 4, pp. 2050–2065, Apr. 2015.
[15] G. Ferraioli, C. A. Deledalle, L. Denis, and F. Tupin, "PARISAR: Patch-based estimation and regularized inversion for multibaseline SAR interferometry," *IEEE Trans. Geosci. Remote Sen.*, vol. 56, no. 3, pp. 1626–1636, Mar. 2018.
[16] F. Chen *et al.*, "Understanding the relationship between the water crisis and sustainability of the Angkor World Heritage site," *Remote Sens. Environ.*, vol. 232, 2019, Art. no. 111293.
[17] H. Tao, M. Li, M. Wang, and G. Lü, "Genetic algorithm-based method for forest type classification using multi-temporal NDVI from Landsat TM imagery," *Ann. GIS*, vol. 25, pp. 33–43, 2019.
[18] H. Xu, F. Chen, P. Tang, and D. Zhang, "Error correction of TOPS Sentinel-1 interferograms," (in Chinese), *Bull. Surv. Mapping*, vol. O, no. 10, pp. 114–118, 2019.
[19] C. Yu, Z. Li, N. Penna, and P. Crippa, "Generic atmospheric correction model for interferometric synthetic aperture radar observations," *J. Geophys. Res.-Solid Earth*, vol. 123, no. 10, pp. 9202–9222, 2018.
[20] R. Lanari, O. Mora, and M. Manunta, "A small-baseline approach for investigating deformations on full-resolution differential SAR interferograms," *IEEE Trans. Geosci. Remote Sens.*, vol. 42, no. 7, pp. 1377–1386, Jul. 2004.
[21] P. Shanker, F. Casu, H. A. Zebker, and R. Lanari, "Comparison of persistent scatterers and small baseline time-series InSAR results: A case study of the San Francisco Bay Area," *IEEE Geosci. Remote Sens. Lett.*, vol. 8, no. 4, pp. 592–596, Jul. 2011.
[22] P. Agram, R. Jolivet, and M. Simons, *Generic InSAR Analysis Toolbox (GIAnT) - User Guide*, 2012. [Online]. Available: http://earthdef.caltech.edu
[23] J. Richards, H. Viles, and Q. Guo, "The importance of wind as a driver of earthen heritage deterioration in dryland environments," *Geomorphology*, vol. 369, Aug. 2020, Art. no. 107363.
[24] X. Shi *et al.*, "Estimation of environmental exposure: Interpolation, kernel density estimation or snapshotting," *Ann. GIS*, vol. 25, pp. 1–8, 2019.
[25] J. Chen *et al.*, "Stereo mapping of Ming Great Wall with remote sensing," *Chin. Sci. Bull.*, vol. 55, no. 21, pp. 2290–2294, 2010.
[26] X. Li, H. Gong, O. Zhang, W. Zhang, and Y. Sun, "Res. on the damage of the Great Wall of Ming Dynasty in Beijing by remote sens.," *Sci. China Ser. E: Technol. Sci.*, vol. 51, Suppl. 1, pp. 195–202, 2008.
[27] M. Manunta *et al.*, "The parallel SBAS approach for Sentinel-1 interferometric wide swath deformation time-series generation: Algorithm description and products quality assessment," *IEEE Trans. Geosci. Remote Sens.*, vol. 57, no. 9, pp. 6259–6281, Sep. 2019.

Fulong Chen received the B.E. degree in surveying and mapping engineering from Wuhan University, Wuhan, China, in 2003, and the Ph.D. degree in cartography and geographical information system from Graduate University of Chinese Academy of Sciences, Beijing, China, in 2008.

He is a Full Professor and Division Director with the Key Laboratory of Digital Earth Science, Aerospace Information Research Institute, Chinese Academy of Sciences, Beijing, China. He is also the Deputy Director with International Centre on Space Technologies for Natural and Cultural Heritage under the Auspices of UNESCO, Beijing, China. His current research interests include synthetic aperture radar for archaeology, interferometric SAR for geohazards and cultural applications, which are the areas where he has four patents and more than 80 academic papers.

Wei Zhou received the B.E. and M.A.E. degrees in photogrammetry and remote sensing from Wuhan University, Wuhan, China, in 2005 and 2008, respectively, and the Ph.D. degree in cartography and geographical information system from University of Chinese Academy of Sciences, Beijing, China, in 2017.

She is an Assistant Professor with the Key Laboratory of Digital Earth Science, Aerospace Information Research Institute, Chinese Academy of Sciences, Beijing, China. Her current research interests include interferometric SAR for cultural heritage monitoring and LiDAR for digital heritage.

Hang Xu received the B.E.degree in remote sensing information and technology from the Capital Normal University, Beijing, China, in 2018. He is currently working toward the M.A.E. degree in surveying and mapping engineering at the Key Laboratory of Digital Earth Science, Aerospace Information Research Institute, Chinese Academy of Sciences, Beijing, China.

His current research interests include the algorithm development of multitemporal InSAR and its applications in preventive monitoring and sustainable conservation of architectural heritage.

Issaak Parcharidis received the B.Sc. degree in geological sciences from the University of Parma, Parma, Italy, in 1984, and the Ph.D. degree in geological sciences from the Agricultural University of Athens, Laboratory of Geology, Athens, Greece, in 1994.

He is a Professor in remote sensing with the Department of Geography, Harokopio University of Athens, Athens, Greece. His main scientific expertise concerns the use of space earth observation systems, specifically synthetic aperture radar interferometry, and very high spatial resolution remotely sensing data for natural disaster and cultural heritage monitoring and assessment.

Hui Lin (Senior Member, IEEE) received the Diploma degree in aerophotogrammetry engineering from the Wuhan Technical University of Surveying and Mapping, Wuhan, China, in 1980, the M.Sc. degree in cartography and remote sensing from the Chinese Academy of Sciences, Beijing, China, in 1983, and the M.A. and Ph.D. degrees in geographic information systems from the University at Buffalo, Buffalo, NY, USA, in 1987 and 1992, respectively.

Since 1993, he has been with the Chinese University of Hong Kong, Sha Tin, Hong Kong, where he is the Chen Shupeng Professor of Geoinformation Science and the Director with Institute of Space and Earth Information Science, Hong Kong. He is currently the Dean of the School of Geography and Environment, Jiangxi Normal University, Nanchang, China. He has authored or coauthored more than 200 academic papers, 10 books, and 1 atlas, and edited 10 conference proceedings. His major research interests include satellite remote sensing for cloudy and rainy environments, virtual geographic environments, and geographic information system applications.

Dr. Lin is the founding President of the International Association of Chinese Professionals in Geographic Information Science. He has been elected as an Academician of the International Eurasian Academy of Sciences and the Vice Chairman of the China National Committee of International Society of Digital Earth. He is the Chief Editor for the *International Journal Annals of GIS*.

Chaoyang Fang received the B.E. degree in metallic materials from Xi'an University of Technology, Xi'an, China, in 1991, the M.Sc. degree in physical oceanography from Ocean University of China, Qingdao, China, in 2002, and the Ph.D. degree in mapping and geographic information system from Ocean University of China, Qingdao, China, in 2005.

He is a Full Professor with the School of Geography and Environment, Jiangxi Normal University, Nanchang, China. He is also the Executive Deputy Director with the Key Laboratory of Poyang Lake Wetland and Watershed Research, Ministry of Education, Jiangxi Normal University. His major research interests include virtual geographic environments, geographic information system applications, and smart city.